Exploring the structural properties and enhancement of Opto-electrical investigations for the synthesized epoxy based polymers with local nanoscale structures

Wissal Jilani[1,2], **Najla Fourati**[3], **Chouki Zerrouki**[3], **Pierre-Antoine Faugeras**[4], **Alain Guinault**[5], **Rachida Zerrouki**[4,6] **and Hajer Guermazi**[2]

[1] Department of Physics, Faculty of Sciences and Arts Dhahran Al Janoub, King Khalid University, PO Box 9004, Abha, Saudi Arabia
[2] Research Unit Physics of Insulating and Semi-Insulating Materials, Faculty of Sciences of Sfax, B.P. 1171, 3000 Sfax, University of Sfax Tunisia, Tunisia
[3] SATIE, UMR 8029 CNRS, ENS Cachan, Cnam, 292 Road Saint Martin, 75003, Paris, France
[4] Laboratory of Chemistry of Natural Substances (EA1069), University of Limoges, Faculty of Science and Technology, 123 Road Albert Thomas, 87060, Limoges, Paris, France
[5] PIMM, Arts et Métiers ParisTech/CNRS/Cnam, 151 boulevard de l'Hôpital, 75013, Paris, France
[6] Centre de recherche sur les matériaux lignocellulosiques, Université du Québec à Trois-Rivières, 3351 boul. des Forges C.P. 500(QC), G9A 5H7 Trois-Rivières, Canada

E-mail: jilaniwissal@yahoo.fr

Keywords: synthesis epoxy resin, interfacial relaxations, optical parameters

Abstract

Epoxy networks of the diglycidyl ether of bisphenol A (DGEBA) were prepared using 4, 4′-diaminodiphenyl (44′DDS) and 3, 3′-diaminodiphenyl (33′DDS) sulfone diamines crosslinking hardeners. The structural, linear optical and mechanical properties of the investigated sample were analysed. Dynamic Mechanical Thermal Analysis and wide-angle x-ray diffraction were conducted to select a candidate presenting interesting thermo-mechanical properties and particular nanostructures embedded in an amorphous matrix. Our choice is therefore focused on DGEBA/33′DDS polymer for which, rocking curve measurements revealed the existence of two principal reflecting planes inclined to each other by about 0.27°. To highlight the potential effect of these interfaces, Thermally Stimulated Depolarization Current (TSDC) and Time Domain Spectroscopy measurements have been carried out. The application of the windowing polarization TSDC technique, in DGEBA/33′DDS polymer sample, gives an almost linear variation of the activation energies in the range between 3.65 and 4.09 eV. To our knowledge, this is the first study concerning epoxy polymers in which activation energies associated to ρ interfacial charge relaxations are calculated. To study the effect of the interfaces and trapped charge carriers, correlated by the angle x-ray diffraction measurements, the optical parameters were investigated. Our contribution will open a new avenue for developing the DGEBA/33′DDS polymer sustainable candidate in optoelectronic engineering applications.

1. Introduction

Recently, epoxy resins are one of the most important classes of thermosetting resins and are extensively used in many fields such as adhesion, heat and corrosion resistance as well as mechanical and electrical properties. Epoxy resins are used in protective coatings, structural applications such as laminates and composites, tooling, construction bonding and adhesives apart from several other less frequent applications. Epoxy resins based on the diglycidyl ether of Bisphenol A (DGEBA) are treated as a modeling system to study epoxy networks by simple aromatic amines. Due to their high strength, low creep, very low shrinkage and good performance at high temperatures, epoxy polymers are widely used in industry, as adhesives, surface coatings and as matrixes for fiber-reinforced plastics. It is important to improve flame resistance and thermal resistance to the application of epoxy resins as electronic materials and in the aerospace industry as matrices for composites. More recently,

epoxy resins are being increasingly used as polymer matrix where nanoparticles or carbon nanotubes have been incorporated [1–3]. Manipulations of the chemical structure and polymerization process allow epoxy resins to span a wide range of mechanical properties, from relatively flexible to very stiff and relatively soft to very hard. Curing of epoxy prepolymer is the most important phase in the fabrication process of epoxy polymers. Electrical insulation, extremely high optical clarity, chemical resistance, adhesive strength and heat resistance properties have changed based on chemical composition of the curing agent and the preparation conditions [4]. Optical properties of polymers have attracted significant attention due to their remarkable technological and optoelectronics applications [5]. The investigation of optical properties of polymers such as refractive index, optical band gap and extinction coefficient have played a key role in optical applications [6].

Epoxy or epoxied resins are well known polymeric materials. It is defined as crosslinked polymers in which the crosslinking is derived from the reactions of epoxy group. The default high performance epoxy resin, diglycidyl ether of bisphenol A (DGEBA), is used in a wide variety of devices, including as the matrix phase in composite systems. The diaminodiphenyl sulfone (DDS) specifically intended for curing epoxy resins is available as two different isomers where the substituents on the two phenylene rings are either in a meta-meta or a para-para arrangement. Curing agents have two or more reactive groups (i.e. Diamines and acid anhydrides) in a molecule, which can react with epoxy groups in which play an important role of applications of epoxy polymers. Aromatic diamines improve thermal, chemical, mechanical and optical properties of the cured epoxy resin in comparison with the aliphatic ones [7]. A number of studies have been performed to examine the effects of crosslinking on the local sub-Tg relaxations of epoxy–amine networks using different techniques such as dielectric spectroscopy [8, 9] dynamic mechanical analysis (DMA) [10, 11] and nuclear magnetic resonance spectroscopy [12, 13]. Crosslink density is an important structural parameter that has a significant effect on the behaviour of a network. J Zhao *et al* found that the crosslink density strongly affects the mechanical response of the amorphous polymers [14]. A sub-T_g γ relaxation peak shifts to higher frequencies with increasing temperature in Arrhenius fashion for both networks, both processes having the same activation energy and being assigned to phenyl ring flipping in DGEBA chains [15]. Numerous facts relating to the curing of diglycidyl ether of Bisphenol A (DGEBA) epoxy prepolymer with 4,4′-diaminodiphenyl sulfone (44′DDS) [16–19] and 3, 3′-diaminodiphenyl sulfone (33′DDS) [20, 21]. In almost all the cases, DGEBA is supplied by a company and used as received. In our case, we have chosen to prepare the samples using a synthesized epoxy prepolymer. The protocol of synthesize of DGEBA is reported in previous work [22]. The structural and thermo-mechanical properties of DGEBA/Meta versus DGEBA/Para diamine were then investigated by Dynamic Mechanical Thermal Analysis (DMTA) and wide-angle x-ray diffraction. Based on the obtained results, only the DGEBA/33′ DDS polymer has been chosen for further structural, dielectric and optical investigations by means of complementary techniques. Grazing incidence small angle x-ray scattering is able to localize eventual oriented nanostructures in the vicinity of material surface, and thus the eventual interfaces, which can act as traps for charge accumulation [23, 24], affect the electrical behavior of polymer.

Herein, the diglycidyl ether of Bisphenol A (DGEBA) epoxy prepolymer was cured with 4,4′-diaminodiphenyl sulfone (44′DDS) and 3,3′-diaminodiphenyl sulfone (33′DDS) network groups. The physical properties will be studied using thermally stimulated depolarization current (TSDC) and Time Domain Spectroscopy (TDS) measurements in order to characterize the interfacial relaxations. TSDC results were correlated with structural ones. UV–visible absorption data were reported and optical parameters such as refractive index and optical band gap were calculated and discussed based on literature.

2. Polymer preparation

The diglycidylether of bisphenol A (DGEBA) is an organic compound used as constituent of epoxy resins. It was made by dispersing 20 g (87.61 mM) of bisphenol A and 28 ml (357.31 mM) of epichlorohydrin. The reaction mixture was stirred at 70 °C (first step). 18.34 g of NaOH (458.53 mM) is introduced in 80 ml of water. This solution was then added dropwise to the mixture of the first step. The global solution was allowed to stand at room temperature and was extracted with chloroform. Subsequently, it was dried, filtered and concentrated over anhydrous $MgSO_4$ under vacuum, to obtain 34.79 g of the epoxy resin [22].

The 4,4′-diaminodiphenyl sulfone (44′DDS) and 3,3′-diaminodiphenyl sulfone (33′DDS) provided by Sigma Aldrich is chosen as hardener (figure 1). One is dissolved into acetone, and DGEBA is added to the synthesis. The solution was then stirred to obtain a homogenous mixture, which was casted into a silicone mold and dried during 2 h at 56 °C under vacuum to eliminate air bubbles, subsequently dried for 21 h at 120 °C. In the last step, the sample was post curing at 120 °C for one hour. This process allows volume and internal stresses relaxation and has deep effects on the mechanical performance of the realized epoxy polymers [25, 26]. In this work, we have chosen to post-cure the samples at 120 °C during one hour. The thickness of the obtained samples is approximately 2 mm with a diameter of 3 cm.

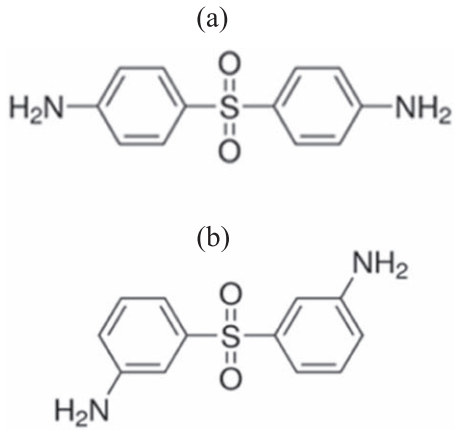

Figure 1. Chemical structure of: (a) 4,4′diaminodiphenylsulfone (44′DDS) and (b) 3,3′diaminodiphenylsulfone (33′DDS).

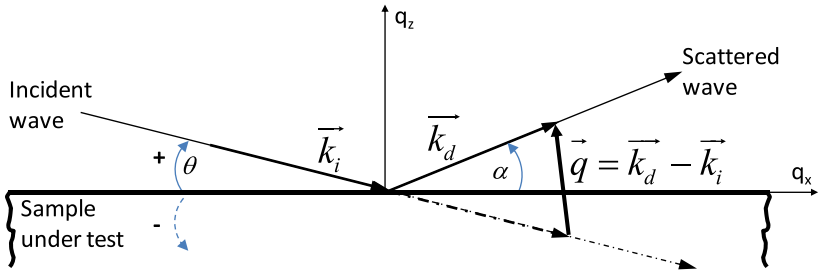

Figure 2. Schematic representation of x-ray measurement setup and the wave vector transfer notation.

3. Characterization techniques

3.1. Fourier transformation infrared analysis

Fourier transform infrared spectroscopy (FTIR) is an analytical technique used to identify the chemical modification of the material. The samples used were prepared as a 5% w/w KBr mixture powder pellet. The FTIR spectra of the epoxy polymers were taken at room temperature (25 °C) using a Perkin Elmer 1000 spectrometer optical cell operated over a spectral range of 4000–400 cm^{-1} at a best resolution of 0.5 cm^{-1}.

3.2. Dynamic mechanical thermal analysis (DMTA)

The specimens of epoxy polymers (30 × 8 × 2 mm^3) were tested at a fixed frequency of 1 Hz in a dynamic mechanical thermal analysis (DMTA) with a Bohlin Instruments apparatus in the 3-point bending mode. DMTA were deformed sinusoidally to a controlled displacement of 0.01 mm. DMTA results were collected during heating cycle in the range 20 to 250 °C with 2 °C min^{-1}. The temperature range was chosen to avoid alteration of the mechanical properties of the investigated polymers. For purposes of analysis, the peak of the loss tangent curve was used as an indicator of the glass transition temperature.

3.3. Grazing incidence x-ray reflectometry

The non-destructive Grazing incidence x-ray reflectometry technique can be probing the polymer from atomic scale to some micrometers [27, 28]. The x-ray source is a tube X with copper anticathode, associated with a silicon crystal as monochromator, to select only Cu $K\alpha 1$ radiation (wavelength of 0.154 nm). The angular divergence of the incident beam, about 0.025°, corresponds to the natural widening of the silicon crystal. The device used comprises two goniometric tables that ensure angular displacements of x-ray source and detector. They move in a coupled or independent way, according to the considered exploration mode (figure 2). This technique explores three modes, rocking-curve, reflectivity and detector scan. The difference between them is related to the values of incidence and scattering angles during the analysis, permitting thus to complementary probe bulk and surface samples. However, a better understanding of the probed layers structure can be done in the reciprocal space, by considering variations of q_x and q_z components of the wave vector transfer $\vec{q} = \vec{k_d} - \vec{k_i}$ where $\vec{k_d}$ and $\vec{k_i}$ are the scattered and the incident wave vectors respectively (figure 2). In this study, we have

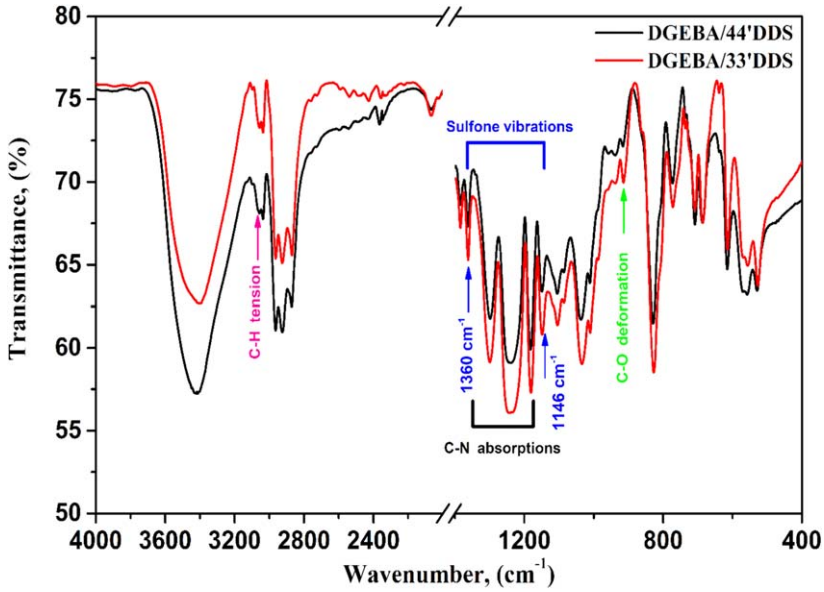

Figure 3. IR spectra of DGEBA/33'DDS and DGEBA/44'DDS polymers.

benefited from x-rays penetration depth and the weak absorption of polymers, to probe epoxy polymers on different thicknesses (in both reflection and transmission modes) according to the incidence angle.

The crystallite size for both epoxy polymers was calculated from x-ray diffraction profiles by measuring the full width at half maximum (FWHM) β (in radian) of the sharp peaks through the Gauss simulation. The Debye Scherrer equation for calculating the crystallite size is given by [29, 30]:

$$D = \frac{k\lambda}{\beta \cos\theta} \tag{1}$$

where k is the Scherrer constant which generally taken to have the value 0.9, λ is the wavelength of light used for the diffraction, and θ the measured angle.

Assuming that the crystallite size and lattice strain have an independent contribution to line broadening, we calculated the strain induced in the epoxy polymer structure with the following relation [29, 30]:

$$\varepsilon = \frac{\beta \cos\theta}{4} \tag{2}$$

The interchain separation length (R) was determined based on the analysis of the most intense crystalline peak from the following Equation [31]:

$$R = \frac{5\lambda}{8 \sin\theta} \tag{3}$$

3.4. Thermally Stimulated Depolarization Current (TSDC) technique

Thermally Stimulated Depolarization Current (TSDC) technique has proven to be a powerful tool especially for the investigation of charge carrier relaxations in dielectric materials. This is an equivalent method of dielectric loss measurements at very low frequencies (10^{-5} to 10^{-2} Hz). This technique enables high resolution and a separation of the processes [32–35]. In this experiment, epoxy polymer samples were coated with 1.5 cm diameter of silver electrodes.

The steps in TSDC measurements of epoxy samples are respectively: (i) the sample was heated at a constant polarization temperature $T_p = 100$ °C and at the applied electric field $E_p = 1.2$ kV mm^{-1} during the time $t_p = 3$ h. (ii) They were then cooled to room temperature (T_0), in the absence of electric field, and were afterward short-circuited for $t_s = 20$ min, to remove eventual surface charges. (iii) After these steps, the samples were reheated at a constant rate of 2 °C mn^{-1} and current peaks were recorded as a function of temperature. The obtained curve represents the TSDC spectrum versus temperature show a peak attributed to the different relaxation processes [36, 37]. To separate partially overlapping relaxations in TSDC spectra, windowing polarization (WP) technique was successfully investigated [38–41].

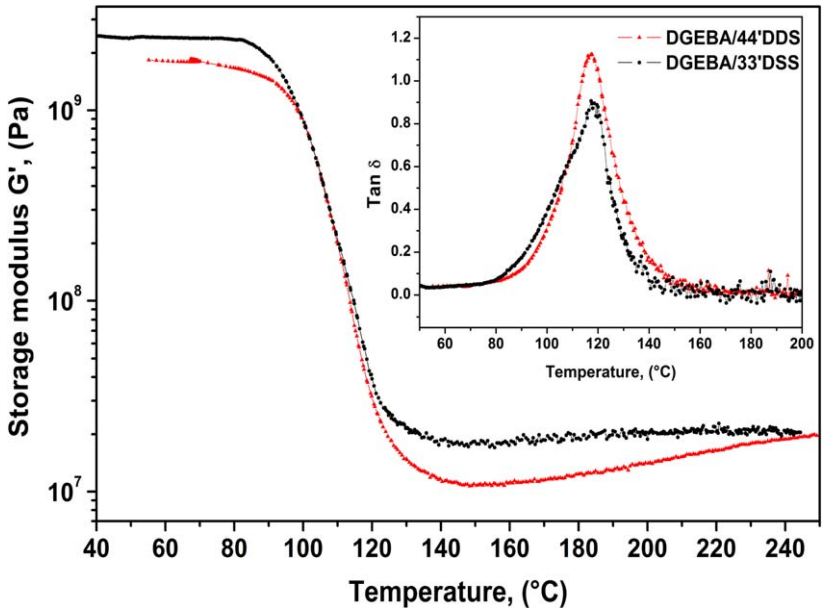

Figure 4. Storage modulus variations versus temperature for DGEBA/33′DDS and DGEBA/44′DDS (the inset represents 'Tan delta' curve).

3.5. Time domain spectroscopy (TDS)

In our case, the prepared epoxy polymer sample was coated with silver electrodes and was sandwiched between two opposing 1.5 cm diameter electrodes of the measuring cell. Then a step voltage equal to 40 V was applied for 100 s carried out using a Keithley 6517 electrometer. After that, the applied voltage was removed and the depolarisation currents versus time were measured during 100 s. By means of Hamon transformation, we calculated the dielectric loss from the experimental transient depolarisation current as following the equation [42]

$$\varepsilon''(f) = \frac{I(t)}{2\pi f V C_0} \tag{4}$$

where I(t) is the depolarisation current, f is the frequency of Hamon ($f = 0.1/t$), C_0 the capacitance of measuring electrodes without the sample and V the applied voltage.

In order to analyse these dielectric relaxations, we used the Havriliak–Negami model to fit correctly the experimental data of the dielectric loss [43]:

$$\varepsilon''(\omega) = (\varepsilon_s - \varepsilon_\infty) r^{-\beta/2} \sin \beta\theta \tag{5}$$

where

$$r = \left[1 + (\omega\tau)^{1-\alpha} \sin\left(\frac{\alpha\pi}{2}\right)\right]^2 + \left[(\omega\tau)^{1-\alpha} \cos\left(\frac{\alpha\pi}{2}\right)\right]^2 \tag{6}$$

$$\theta = \arctan\left[\frac{(\omega\tau)^{1-\alpha} \cos\left(\frac{\alpha\pi}{2}\right)}{1 + (\omega\tau)^{1-\alpha} \sin\left(\frac{\alpha\pi}{2}\right)}\right] \tag{7}$$

where, α is the shape parameter representing symmetrical distribution of relaxation time and β is the shape parameter of an asymmetric relaxation curve of ε'' versus ω peaks and τ is the relaxation time of the system.

3.6. UV–visible spectroscopy

The optical measurements of DGEBA/DDS polymer system were carried out at room temperature using a Perkin Elmer Lambda 950 UV–vis-Near-IR spectrophotometer in the wavelength range from 320 to 1000 nm with a 1 nm interval.

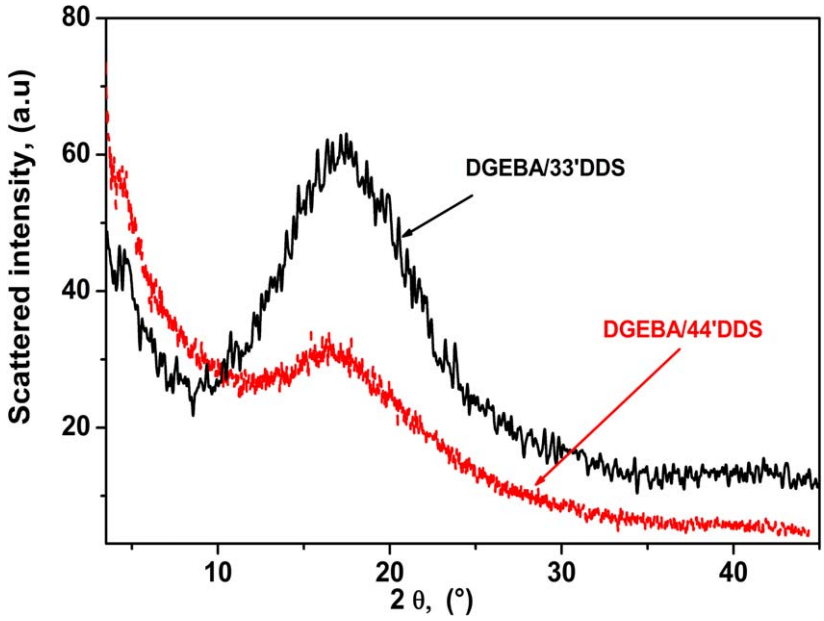

Figure 5. X-ray diffraction patterns of DGEBA/33′DDS and DGEBA/44′DDS polymers.

4. Results and discussion

4.1. FTIR spectra results for DGEBA/DDS polymers

FTIR can provide fundamental information on the molecular structure of organic and inorganic components, and is one of the most versatile analytical techniques for the non-destructive, chemical characterization of geological samples. It can provide information about the nature of interactions in polymer. FTIR measures the vibration and rotation of molecules influenced by infrared radiation at a specific wavelength. Both DGEBA/DDS curing reaction can result of significant changes of the chemical structure of the molecule and these changes may be reflected in the IR spectrum of the system. FTIR spectra of both DGEBA/DDS polymers are presented in figure 3. No differences between the two polymers were detected. Both of them show C–N absorptions in the 1200–1350 cm^{-1} region and sulfone stretching vibrations at 1146 and 1360 cm^{-1} indicating that polymerization has occurred. We noted the N–H stretching band in the 3400–3500 cm^{-1} regions. The weakness of oxirane ring characteristic bands (ν_{CO} at 915 cm^{-1}, attributed to the C–O deformation of the oxirane group which indicates a major portion of the epoxy ring and ν_{CH} at 3057 cm^{-1} attributed to the C–H tension of the methylene group of the epoxy ring) indicates that the polymerization process is completed. This quantitative analysis of the major chemical groups in both epoxy systems, led us to understand not only the reaction mechanism in each system but also the cure kinetics, which showed strong dependence on the formulation of the system.

4.2. DMTA results

The variation of storage modulus G′ versus temperature for DGEBA/33′DDS and DGEBA/44′DDS polymers is plotted in figure 4, where an inset represents 'tan delta' curve. This figure shows that the two polymers have the same Tg value, of about 118 °C. Results indicate that for temperatures well above the glass temperature Tg (the inflexion point of a G′ curve), DGEBA/DDS polymers are in the rubbery state and the storage modulus are consequently very low. When the temperature is much lower than Tg, the storage modulus values are elevated. This can be explained by the fact that at these temperatures, large-scale conformational changes are impossible for polymers and only local conformational changes are allowed. Thus, the stiffness of the material is high and the storage modulus is important [44]. In the temperature ranges from 140 to 240 °C, the sample DGEBA/33′DDS shows a slight increase of storage modulus which various from 1.87×10^7 to 2.07×10^7 Pa. Meanwhile, the sample DGEBA/44′DDS revealed a significant increase of storage modulus from 1.12×10^7 to 1.88×10^7 Pa in the same range. Therefore, the DGEBA/33′DDS polymer seems to have better thermo-mechanical properties as it presents certain stability of storage modulus above T_g. However, further structural characterizations are necessary to validate this choice. X-ray diffraction has thus been investigated.

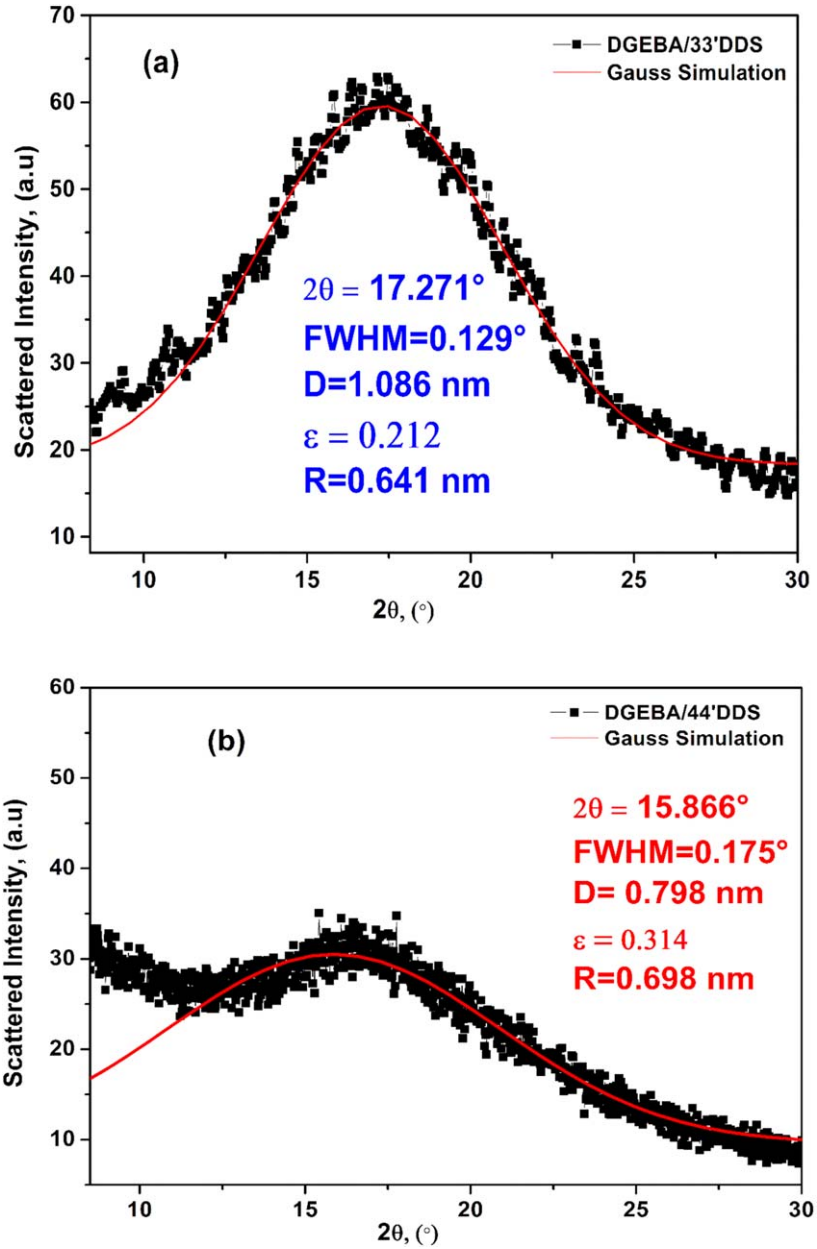

Figure 6. (a) and (b). Crystallite parameters estimated by using Gauss simulation for the spectra of DGEBA/33′DDS and DGEBA/44′ DDS polymers, respectively.

4.3. Structural study

XRD is an important method for studying the internal structure of solid materials. These patterns allow you to know if a material is crystalline or amorphous. Crystalline materials are well-defined for diffraction patterns, whereas amorphous materials have no crystalline peaks.

Figure 5 shows the wide-angle x-ray diffraction patterns of DGEBA/33′DDS and DGEBA/44′DDS polymers.

The diffractograms indicate that both materials are amorphous, since no sharp diffraction peaks are present. Figures 6(a) and (b) shows the crystallite parameters estimated by using Gauss simulation of the spectra for the both samples. Our parameter values are indexed for the spectra of DGEBA/33′DDS and DGEBA/44′DDS polymers, respectively (see figures 6(a) and (b)). For the DGEBA/44′DDS sample, the size of the crystallites was 0.798 nm. However, it has 1.086 nm for the DGEBA/33′DDS epoxy polymer sample. The crystalline size of DGEBA/33′DDS epoxy polymer sample is the largest among DGEBA/44′DDS sample, which favors carriers transfer along the DGEBA epoxy chain.

The broad scattering peaks present a slight difference in their widths and center positions. Based on the Bragg's law, the calculated values of diffracted plans distances in the DGEBA/33′DDS and DGEBA/44′DDS systems, are 0.51 nm and 0.55 nm respectively, with a relative uncertainty of 3.10^{-4} for both. This suggests that

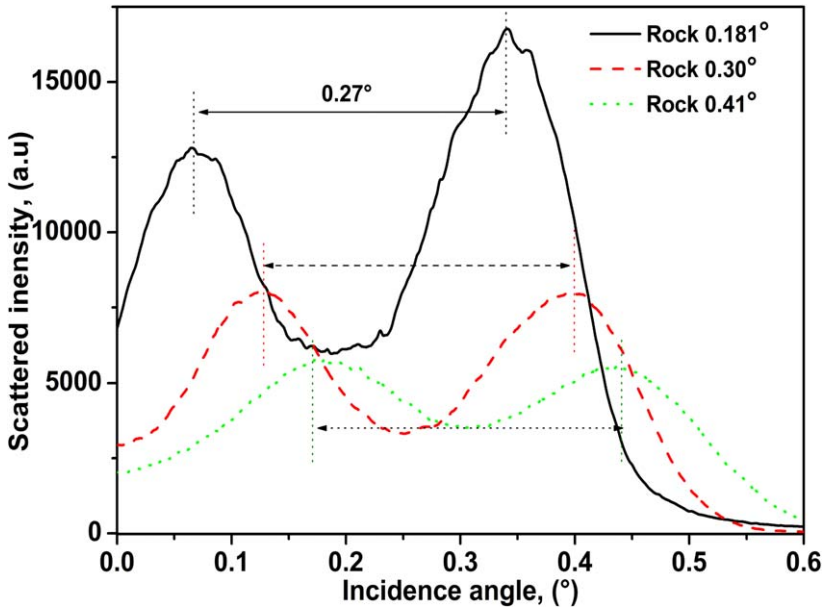

Figure 7. Scattered intensity versus patterns are shifted along the ordinate incidence angles for different exploration ranges.

DGEBA/33′DDS is slightly more 'compacted' (about 8%). These diffraction peaks can be attributed to a local ordered chain that form layers, and the calculated distances correspond to average layer thickness. The difference in the layer thickness between the two DGEBA/DDS polymers is due to the curing agent structure (different para or meta conformation (figure 1). As x ray diffractograms have emphasized some particularities for DGEBA/33′DDS system (higher scattered intensity and lower average layer distance), and due to the fact that this system presents better thermo-mechanical properties, we have focused our interest only on this polymer for further investigations. To further characterize the specific structure of this polymer DGEBA/33′DDS, we performed rocking-curve (RC) and detector scan (DS) measurements. For RC measurements, the source and detector set swivels from $\theta = 0$ to $\theta = \theta_{max}$ (i.e. from $\alpha = \alpha_{max}$ to $\alpha = 0$), while the sum of incidence and scattering angle values is maintained constant ($\theta + \alpha = \theta_{max} = \alpha_{max} =$ constant). In the particular case of polymers, since the x-ray absorption coefficient is small, the material can be considered as 'transparent' for x-rays. Consequently, exploration in RC mode can be started from 'negative' incidence values (the incident beam enters under the surface sample via the edges. See figure 2 for angular orientation) and continued beyond θ_{max}, to access the transmitted parts of scattering. Different values of θ_{max}, 0.18°, 0.30° and 0.41°, have been chosen to access to different values of the q_z component of the wave vector transfer: 0.13 nm^{-1}, 0.21 nm^{-1} and 0.29 nm^{-1} respectively. These values correspond to the spatial frequencies domain where undulations have been observed on reflectivity measurements. Scattered intensities, according to incidence angles are gathered in figure 7. The curves presented an abnormal shape where, instead of specular reflection at $\theta_{max}/2$ and Yoneda's peaks around it, we notice the presence of two important peaks separated by a constant distance. This reveals the existence of two principal reflecting structures, mainly based on planes constituted from the phenyl rings (Scheme 3), which are inclined to each other by about 0.27°.

Detector Scan measurements (figure 8(a)) were carried out for scattering angles ranged between −0.5° and 1° (the 'negative' values of α correspond to the scattered transmission, while the scattered reflection is obtained for the positive values). We have chosen four grazing incidences, 0.05°, 0.08°, 0.20° and 0.30°, to explore the samples over different thicknesses (thanks to the penetration depth of x-rays which closely depends on incidence angle value). Only parts of the sample close to the surface are analyzed for the two first incidences, while deeper layers are concerned for the two others. For all incidences, we observe the presence of some broad peaks.

To compare the four DS measurements, x-ray scattered intensity is represented as a function of q_z component rather than scattering angles (figure 8(b)). For 0.05° and 0.08° incidence angles, the presence of broad peaks around $q_z = 0.175$ nm^{-1} and $q_z = 0.386$ nm^{-1} are signs of localized periodic structures whose periodicity is about 36 nm. For 0.2° incidence, the main peak shifts slightly towards lower values of q_z, while the second one disappears. This means that the periodic structure becomes somewhat more spaced (about 42 nm) in deeper parts. Figure 8(b) shows also that the intensity level is reduced for the incidence of 0.3° for which the probed layers are increasingly deeper. The presence of peaks at lower q_z values confirms the fact that periodicity of structure increases, as one moves away from the surface layers (structure's period of order of 64 nm in this case). This difference between surface layers and deeper ones can be explained by the fact that the polymerization

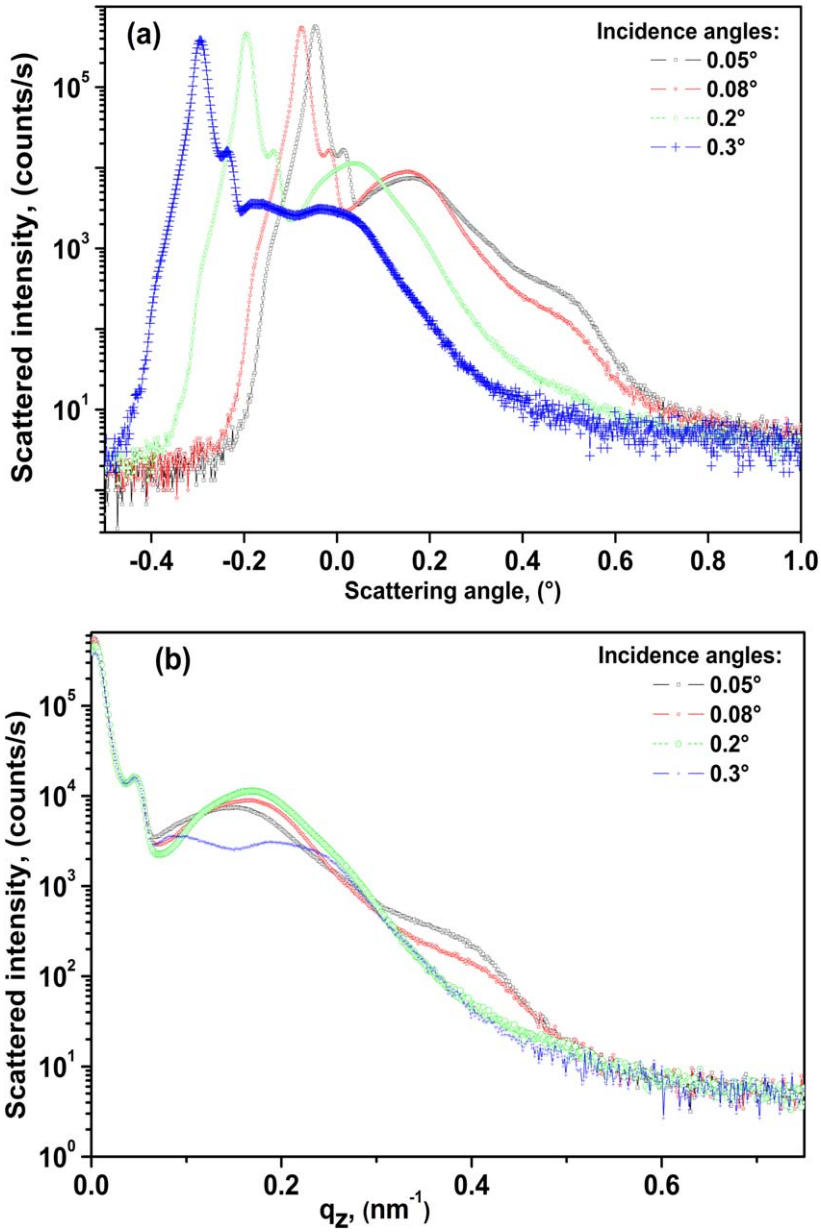

Figure 8. Detector scan measurements for different incidence angles: (a) scattered intensity versus scattering angle, (b) the q_z component of the wave vector transfer.

phenomenon takes place first at the surface and then progressively in the bulk of the material [27]. The localized oriented nanostructures, which exist in the amorphous material, can lead to some interfaces able to trap charges carriers which can affect the electrical and optical properties of such polymer.

To highlight the potential effect of these interfaces on space charge relaxations, TSDC measurements with WP technique have been carried out on the DGEBA/33′DDS polymer.

4.4. Dielectric characterization

In TSDC measurements we have proceeded to windowing polarization to access only interfacial relaxations in the material. TSDC curve recorded after WP poling at 100 °C is presented in figure 9. Experimental curve has been fitted using Cresswell and Perlman model [45], and the obtained 'theoretical' curve is added in the same figure (solid line).

The recorded current was then fitted using Cresswell and Perlman model [45]:

$$I(T) = A \exp\left[-\frac{E_a}{K_B T} - \frac{1}{q\tau_0}\int_{T_0}^{T} \exp\left(-\frac{E_a}{K_B T'}\right)dT'\right] \tag{8}$$

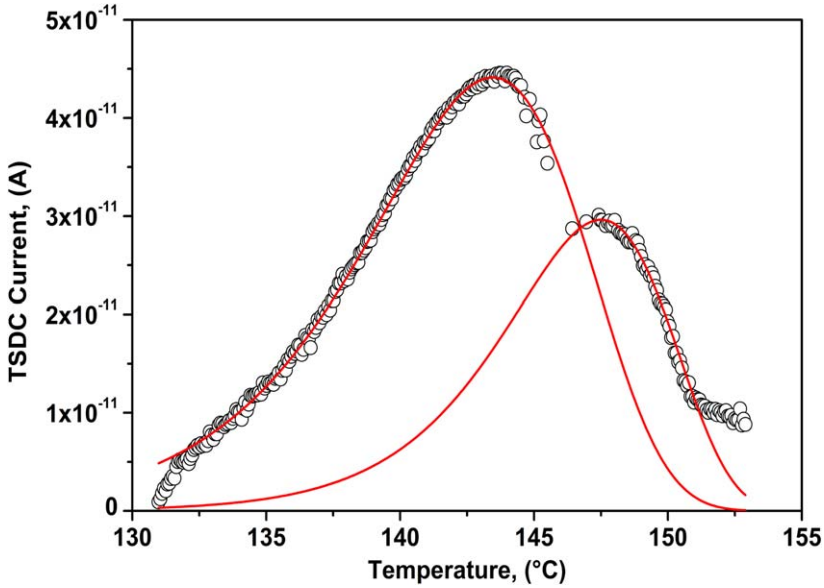

Figure 9. TSDC current of windowing polarization for ρ relaxation (Tp = 100 °C).

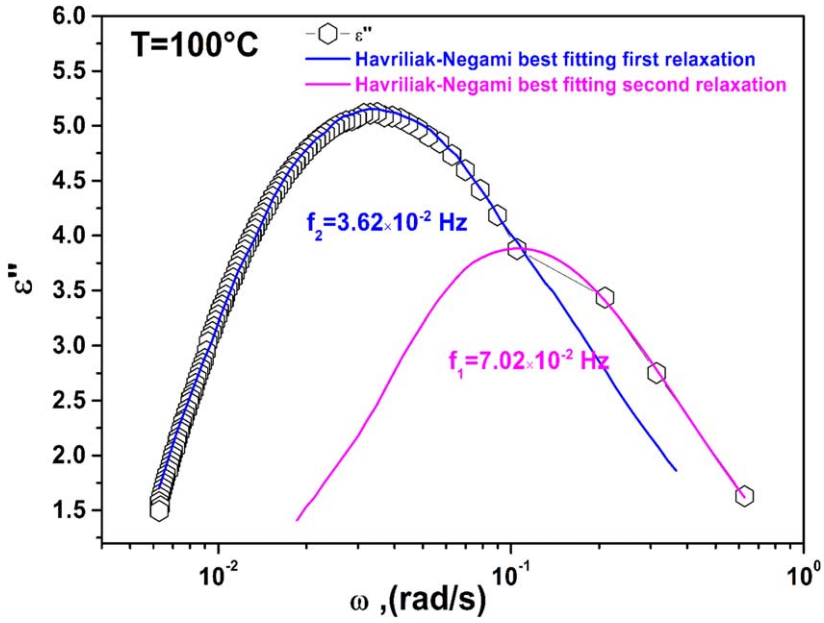

Figure 10. Evaluation of dielectric loss (ε'') data measured partly in the time domain derived from Hamon transform of discharge current after poling at 40 V by fitting Havriliak-Negami function.

Where $\mathbf{T_0}$ A is the factor pre-exponential, E_a relies the activation energy, k_B represents the constant of Boltzmann, q is the heating rate, T_0 is the initial temperature, T is the temperature at time t and τ_0 is the relaxation time at T_0.

The WP-TSDC was well fitted by two peaks (figure 9). The first peak was attributed to the release of charges accumulated at the interfaces formed in the bulk of this polymer, already detected by reflectometry results. So, the second peak can be due to relaxation of charges accumulated in the material electrode interfaces.

The activation energies E_a estimated from the considered model are equal to 3.65 and 4.09 eV.

In order to confirm the interfacial relaxations, we calculated the dielectric loss factor from transient current data via Hamon transformation, since it is well known that this relaxation generally appears in very low frequency domain, which cannot be often accessible by direct dielectric measurements. Figure 10 displays the dielectric loss plot versus frequency. It shows a very broad peak with a shoulder at high frequencies, that confirms the two interfacial relaxations due to release of charges trapped at the interfaces metal-polymer and

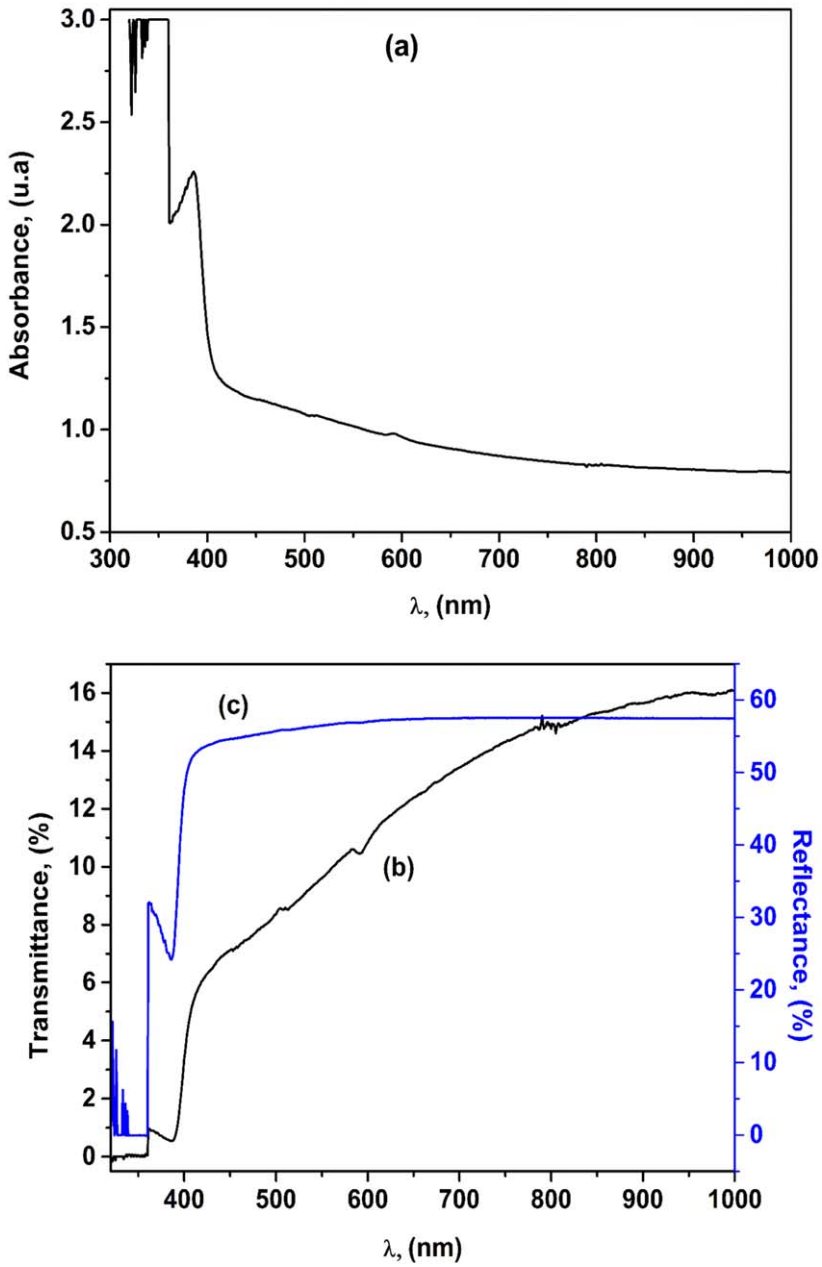

Figure 11. Absorbance (a), transmittance (b) and reflectance (c) spectra of DGEBA/33′DDS.

internal one in the bulk. The Havriliak-Negami equation is fitted to the experimental data of the figure 10 and the relaxation time (τ) at peak maximum was extracted. The frequencies at maximum dielectric loss (ε'') for the tow interfacial relaxations f_1 and f_2 are deduced using the relaxation time formula $\tau = 1/(2\pi f)$. The values of frequencies of the two investigated interfacial relaxations are indexed on figure 10. Indeed, x ray analysis demonstrates the presence of local periodic nanosized states in the polymer which act as interfaces and constitute deep charge carrier traps. In addition, their periodicity increases with increasing distance to the surface of the sample. Thus, a distribution of trap levels was created, resulting in a distribution of relaxation times of the accumulated charges. The same results were observed in this polymer at various temperatures (−100 to 100 °C) as reported in previous work [46].

4.5. Optical characterization

For further investigations of the effect of interfaces and trapped charge carriers already emphasized by x-ray and dielectric characterizations, we have investigated the optical properties of the polymer DGEBA/33′DDS, by absorption measurements. Figure 11 shows the absorbance (a), transmittance (b) and reflectance (c) spectra of the polymer. It shows high UV-light absorption. An absorption peak is observed at 380 nm, related to n - Π^* HOMO-LUMO transition in the benzene rings. This peak was detected in other works [47, 48]. Then a sharp

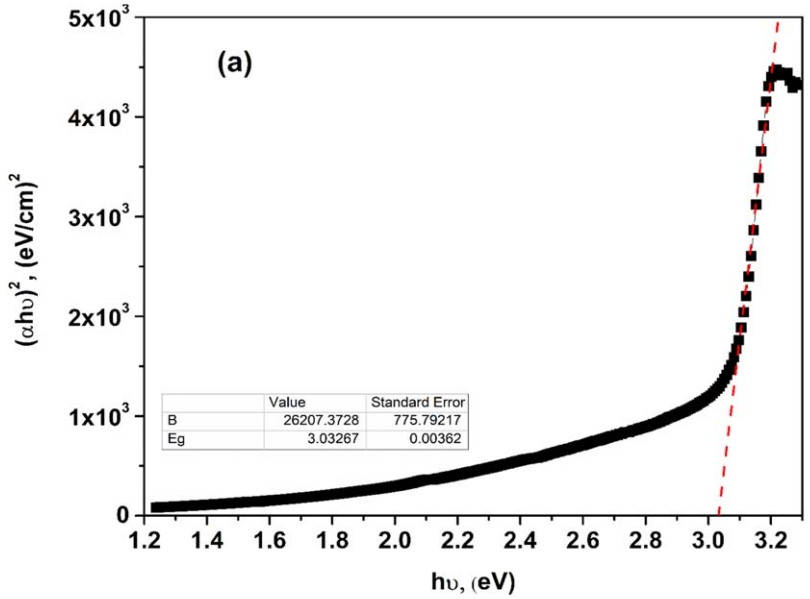

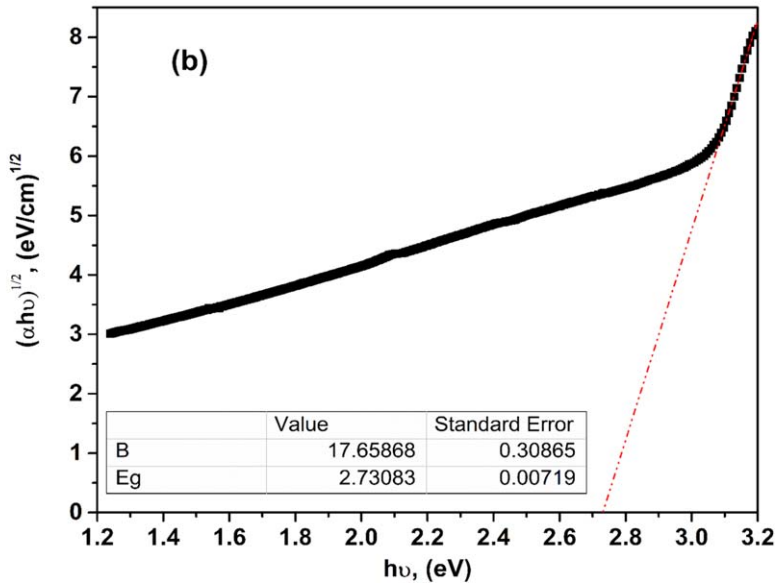

Figure 12. The direct (a) and indirect (b) band gap energy for DGEBA/33′DDS using Tauc's model (red dash line).

absorption edge takes place due to the band-to-band transition. Furthermore, the DGEBA/33′DDS shows high reflectance of about 58% in the visible-NIR range. The high reflectance values make this polymer suitable for IR shielding coats. Transmittance exhibits slight increase with wavelength but it still lower than 16% transparency. The low transmittance values can be explained by light scattering due to the presence of interfaces in the bulk of this polymer.

According to the Tauc relation, the optical band gap was determined by [49]:

$$(\alpha h\nu) = B(h\nu - E_g)^r \tag{9}$$

where B is a constant which depends on the transition probability, E_g is the band gap energy, $h\upsilon$ is the incident photon energy and r is an exponent characteristic of optical transition which can take the values 1/2 or 2 for allowed direct and indirect transitions respectively.

The optical band gap energy has been calculated by plotting $(\alpha h\upsilon)^r$ versus $h\upsilon$ and taking intercepts on the energy axis of the extensions along the linear portion of energy curves, via the fitting using Tauc's model, as shown in figures 12(a) and (b). The calculated values of the direct and indirect band gaps are found to be 3.032 and 2.730 eV with standard error 0.0036 and 0.0071 eV, respectively.

The refractive index (n) is associated to the dispersion behavior below the inter-band absorption edge corresponds to the fundamental electronic excitation. It is an important parameter for optoelectronic technologies. It is significant to determine optical parameters of polymer. n is calculated from the following

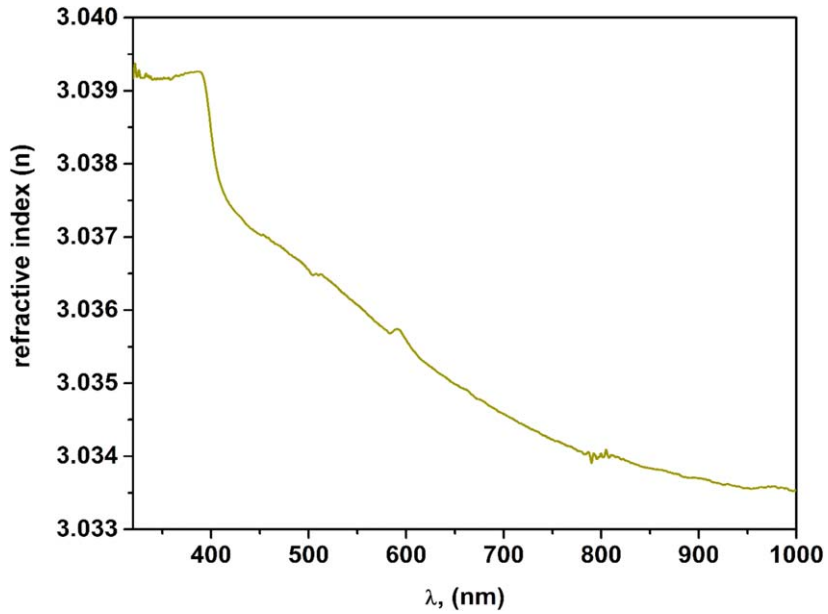

Figure 13. The refraction index as a function of wavelength.

equation [47, 48]:

$$n = \frac{1+R}{1-R} + \sqrt{\frac{(1+R)^2}{(1-R)^2} - (k^2 - 1)} \tag{10}$$

where R is the calculated reflectance, $k = \frac{\lambda\alpha}{4\pi}$ is the extinction coefficient, $\alpha = 2.303A/d$ is the absorption coefficient, d is the thickness of the sample and A is the absorbance. As seen in figure 13, the refractive index decreases with increasing wavelength. The refractive index of the investigated sample is completely depending on the absorption coefficient. The high refractive index makes the epoxy polymer suitable for applications like waveguide-based optical circuits, when W F Ho *et al*, investigate and report the stability and optical characterizations of a modified organometallic high refractive index polymer film in manufacturing of optical waveguide devices [50]. The refractive index changes with the variation of the wavelength of the incident light beam due to these interactions, i.e. the optical loss caused by absorption and scattering, which decreases the amplitudes of the transmission intensity oscillations at shorter wavelengths.

The real (ε') and imaginary (ε'') parts of the permittivity are related to (n) and (k) values throughout the formulas [47, 48]:

$$\varepsilon' = n^2 - k^2 \tag{11}$$

$$\varepsilon'' = 2nk \tag{12}$$

Figures 14 (a) and (b) shows dependence on wavelength of real (ε') and imaginary (ε'') parts of dielectric constant. As seen in this figure, the optical losses ε'' increases with the rise of wavelength in the visible-NIR region. While (ε') decreases when the wavelength increases.

The high values of ε' can be related to the presence of the interfaces within the material as demonstrated by x-ray investigations. This property makes the DGEBA/33′DDS epoxy polymer suitable candidate used in high-performance embedded capacitors. It is found that in infrared range the dispersion of ε' is linear as a function of the square of the wavelength (λ^2) (insert of figure 14(a)), while ε'' is linear with λ^3(insert of figure 14(b)). This behavior is in good agreement with the classical theory of the dielectric constant which is expressed by the following relation in the near infrared region ($\omega\tau \gg 1$) [47]:

$$\varepsilon_1 \approx \varepsilon_\infty - \frac{\varepsilon_\infty \omega_p^2}{4\pi^2 c^2}\lambda^2 \tag{13}$$

$$\varepsilon_2 \approx \varepsilon_\infty \frac{\varepsilon_\infty \omega_p^2}{8\pi^3 c^3 \tau}\lambda^3 \tag{14}$$

Where ε_∞ is the dielectric constant at high frequencies, ω_p the pulsation of plasma, τ the relaxation time and C is the speed of light in vacuum.

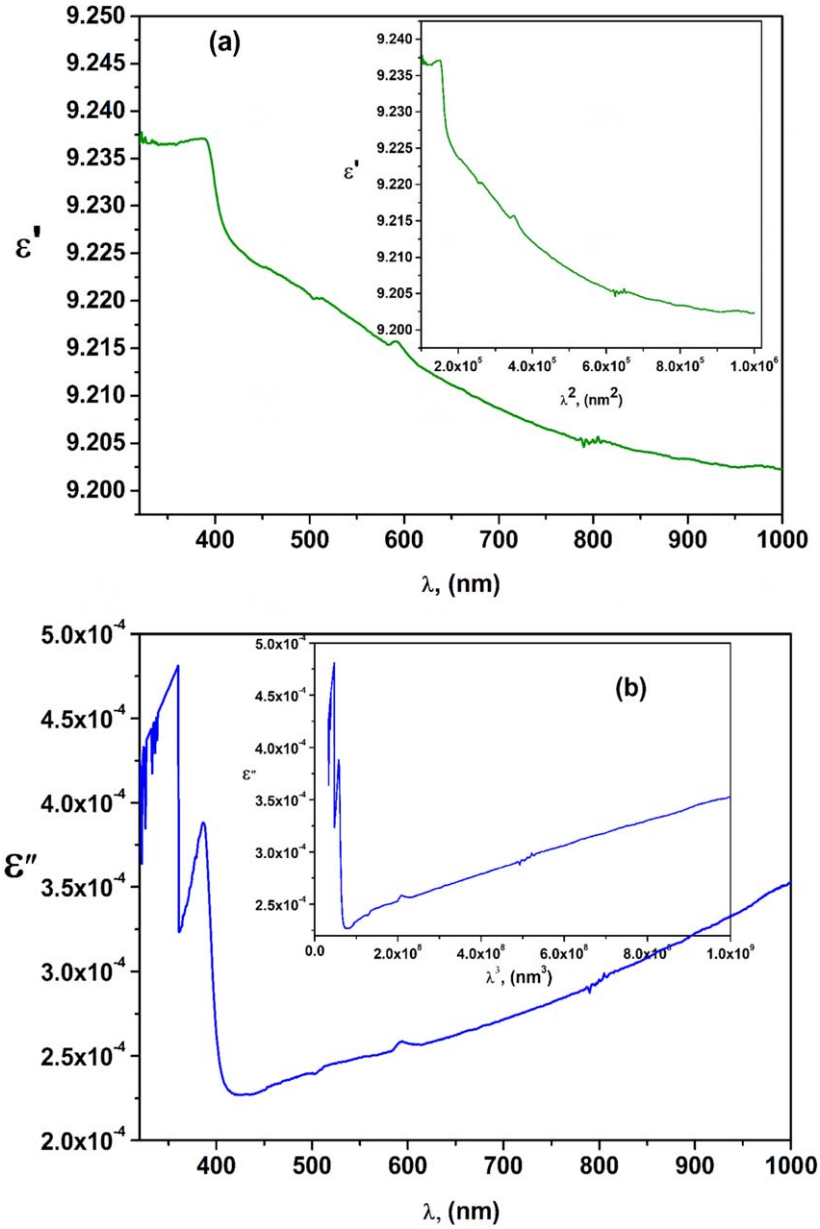

Figure 14. (a) and (b). Real and imaginary parts of dielectric constant versus wavelength (the inset represents real part versus λ^2 and imaginary part versus λ^3, respectively.

Table 1. Calculated values of optical constants deduced from dielectric permittivity's.

ε_∞	$(\omega_p \times 10^{14})$, (rad/s)	$(\tau \times 10^{-14})$, (s)	$(N/m_e^*(\times 10^{44}))$, $(g^{-1}cm^{-3})$
9.22	6.59	4.76	11.03

The free carrier concentration to effective mass ratio N/m_e^* is calculated from the following relation [47]:

$$\omega_p^2 = \frac{4\pi Ne^2}{\varepsilon_\infty m_e^*} \tag{15}$$

The obtained values are listed in table 1.

As seen from table 1, the plasma frequency ω_p is proportional to the electron density. In DGEBA/33′DDS epoxy polymer, the densities are such that ω_p falls into the high visible or ultraviolet range. We find that the variation in optical constant values for DGEBA/33′DDS epoxy polymer are comparable to the range of values

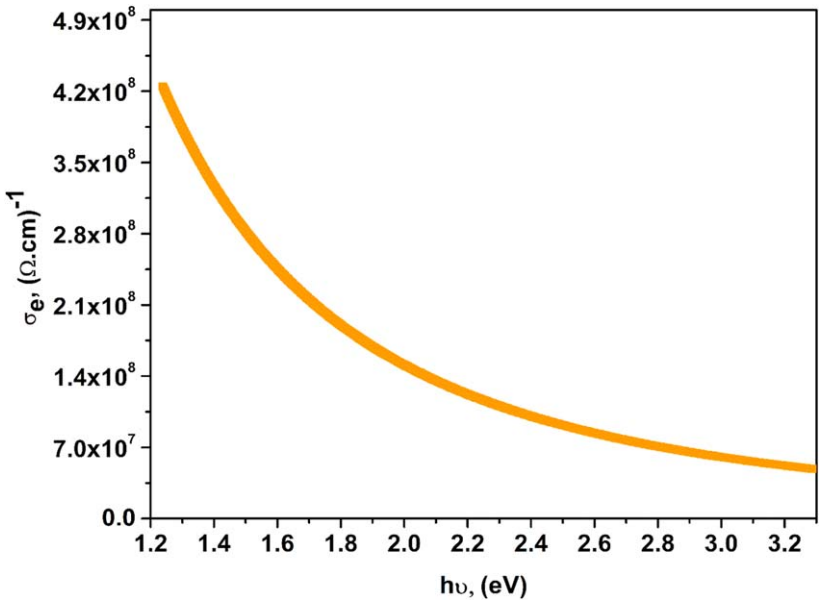

Figure 15. Electric conductivity σ_e versus $h\upsilon$ photon energy.

reported by A. Bouzidi *et al*, when studied the effect of the different concentrations of ZnO:Mn incorporation on the epoxy nanocomposites [51]. At very high frequencies, their optical constants are like those of insulator system for the investigated DGEBA/33′DDS epoxy polymer sample.

The electric conductivity is calculated using the equation:

$$\sigma_e = \frac{2\lambda\sigma_{op}}{\alpha} \tag{16}$$

where σ_{opt} is the optical conductivity $\sigma_{op} = \frac{\alpha\lambda c}{4\pi}$. Figure 15 shows the variation of electrical conductivity with respect to photon energy. The electrical conductivity for the DGEBA/33′DDS epoxy polymer sample gradually decreases when the photon energy increase. The high electrical conductivity observed for DGEBA/33′DDS epoxy polymer sample, in the lower photon energy, confirms the high photo response which related to the high absorbance and to the electron excitation by the photon. The results were similar to those reported in the literature [52].

The high values of σ_e in the visible-NIR region can be explained by the high concentration of charges carriers.

5. Conclusion

The DGEBA epoxy prepolymer cured with 4,4′-diaminodiphenyl sulfone (44′DDS) and 3,3′-diaminodiphenyl sulfone (33′DDS) as hardeners were synthesized to study the curing behavior and performance. Their structural, linear optical and mechanical properties were analysed and investigated by several techniques. A significant difference between the two polymers is revealed by the DMTA measurements. The DGEBA/33′DDS polymer was found to have the best thermo-mechanical properties. The wide-angle x-ray diffraction measurements also showed a difference between the two polymers, as the DGEBA/33′DDS system presented the higher scattered intensity and the lower average layers distances, therefore this polymer is more compact than that cured with 44′ DDS. Small angles x-ray scattering measurements have consequently been performed for the DGEBA/33′DDS. All measurements demonstrate that this polymer presents some localized periodic nanostructures whose periodicity (≈36 nm for the surface layers) increases as one moves away from the surface and penetrates inside the material. These localized oriented nanostructures in the vicinity of amorphous material surface, constitute deep charge carrier traps, which affect the electrical properties of such polymer. This has been confirmed by dielectric measurements, where two interfacial space charge relaxations were observed (the activation energies calculated for the two regions of the interfacial relaxations are 3.65 eV and 4.09 eV, respectively). Moreover, the optical properties of DGEBA/33′DDS epoxy polymer were investigated using UV–vis-NIR absorption measurements. Results show that this polymer has high refractive index *n* and high dielectric permittivity. The high electrical conductivity in the lower photon energy confirms the high photo response of the DGEBA/33′

DDS epoxy polymer. We conclude that DGEBA/33′DDS epoxy polymer sample, based on the investigated properties, is a highly suitable candidate in optoelectronic engineering applications.

Conflicts of interest

No conflicts of interest exist.

ORCID iDs

Wissal Jilani https://orcid.org/0000-0002-4651-7270

References

[1] Hendra S, Jaafar S and Sulong A 2013 Electrical conductivity and hardness property of CNTs/epoxy nanocomposites *Adv. Mat. Res.* **701** 197–201
[2] Patsidis A C, Kalaitzidou K and Psarras G C 2013 Carbon or barium titanate reinforced epoxy resin nanocomposites: dielectric, thermomechanical and functional behaviour *J. Adv. Phys.* **21** 7–12
[3] Macutkevic J, Kuzhir P P, Paddubskaya A G, Banys J, Maksimenko S A, Stefanutti E, Micciulla F and Bellucci S 2013 Broadband dielectric/electric properties of epoxy thin films filled with multi-walled carbon nanotubes *J. Nanophotonics* **7** 073593-1-073593-14
[4] Ramesh P, Ravikumar L and Burkanudeen A 2014 Curing properties of novel curing agent based on phenyl bisthiourea for an epoxy resin system *J. Therm. Anal. Calorim.* **115** 713–22
[5] Badran H A 2012 Study on optical constants and refractive index dispersion of neutral red doped polymer film *J. Appl. Sci.* **9** 250–3
[6] Neumann H, Horig W, Reccius E, Sobotta H, Schumann B and Kuhn G 1979 Growth and optical properties of $CuGaTe_2$ thin films *Thin Solid Films* **61** 13–22
[7] Ghaemy M, Barghamadi M and Behmadi H 2004 Cure kinetics of epoxy resin and aromatic diamines *J. Appl. Polym. Sci.* **94** 1049–56
[8] Andjelić S, Fitz B and Mijović J 1997 Reorientational dynamics and intermolecular cooperativity in reactive polymers. II. multifunctional epoxy–amine systems *Macromolecules* **30** 5239–48
[9] Pissis P and Fragiadakis D 2007 Dielectric studies of segmental dynamics in epoxy nanocomposites *Journal of Macromolecular Science, Part B* **46** 119–36
[10] Sindt O, Perez J and Gerard J F 1996 Molecular architecture-mechanical behaviour relationships in epoxy networks *Polymer* **37** 2989–97
[11] Heux L, Halary J L, Lauprêtre F and Monnerie L 1997 Dynamic mechanical and 13C n.m.r. investigations of molecular motions involved in the β relaxation of epoxy networks based on DGEBA and aliphatic amines *Polymer* **38** 1767–78
[12] Heux L, Lauprêtre F, Halary J L and Monnerie L 1998 Dynamic mechanical and 13C n.m.r. analyses of the effects of antiplasticization on the β secondary relaxation of aryl-aliphatic epoxy resins *Polymer* **39** 1269–78
[13] Lauprêtre F, Eustache R P and Monnerie L 1995 High-resolution 13C nuclear magnetic resonance investigation of local motions in model epoxy resins *Polymer* **36** 267–74
[14] Zhao J, Yu P and Dong S 2016 The influence of crosslink density on the failure behavior in amorphous polymers by molecular dynamics simulations *Materials* **9** 234
[15] Mohammad K H, Samuel J T, Ahmed A, Jeffrey S W and Kenneth A M 2016 Polymer chain dynamics in epoxy based composites as investigated by broadband dielectric spectroscopy *Arabian J. Chem.* **9** 305–15
[16] Bidstrup S A, Sheppard N F and Senturia S D 1989 Dielectric analysis of the cure of thermosetting epoxy/amine systems *Polym. Eng. Sci.* **29** 325–8
[17] White S R, Mather P T and Smith M J 2002 Characterization of the cure-state of DGEBA-DDS epoxy using ultrasonic, dynamic mechanical, and thermal probes *Polym. Eng. Sci.* **42** 51–67
[18] Burger N, Laachachi A, Mortazavi B, Ferriol M, Lutz M, Toniazzo V and Ruch D 2015 Alignments and network of graphite fillers to improve thermal conductivity of epoxy-based composites *Int. J. Heat. Mass. Tran.* **89** 505–13
[19] Chen H, Cong P, Su C, Huang T and Li T 2014 Mechanical strength and tribological properties of diglycidyl ether of bisphenol-A cured by poly(amide-amidic acid) and 4, 4′-diaminodiphenylsulfone *J. Macromol. Sci. B.* **53** 118–32
[20] Zong L, Zhou S, Sun R, Kempel L C and Hawley M C 2004 Dielectric analysis of a crosslinking epoxy resin at a high microwave frequency *J. Polym. Sci. Pol. Phys.* **42** 2871–7
[21] Hassan M K, Tucker J S, Abukmail A, Wiggins J S and Mauritz K A 2015 Polymer chain dynamics in epoxy based composites as investigated by broadband dielectric spectroscopy *Arabian J. Chem.* **9** 305–15
[22] Jilani W, Mzabi N, Gallot-Lavallée O, Fourati N, Zerrouki C, Zerrouki R and Guermazi H 2015 Study of AC electrical conduction mechanisms in an epoxy polymer *Eur. Phys. J. Plus.* **130** 15235-2-15235-15239
[23] Jilani W, Mzabi N, Fourati N, Zerrouki C, Gallot-Lavallée O, Zerrouki R and Guermazi H 2015 Effects of curing agent on conductivity, structural and dielectric properties of an epoxy polymer *Polymer* **79** 73–81
[24] Smaoui H, Arous M, Guermazi H, Agnel S and Toureille A 2010 Study of relaxations in epoxy polymer by thermally stimulated depolarization current (TSDC) and dielectric relaxation spectroscopy (DRS) *J. Alloy. Compd.* **489** 429–36
[25] Verlag C H 1993 Rosato's plastics encyclopedia and dictionary Reference book (ISBN: 3-446-16490-1)
[26] Williams J and Scardino W 1987 Adhesives selection engineered materials handbook *Composites* 2 (ASM. International.) Reference book (ASM 620.1)
[27] Medhioub H, Zerrouki C, Fourati N, Smaoui H, Guermazi H and Bonnet J J 2007 Towards a structural characterization of an epoxy based polymer using small-angle x ray scattering *J. Appl. Phys.* **101** 0435091–6
[28] Namouchi F, Smaoui H, Guermazi H, Zerrouki C, Fourati N, Agnel S, Toureille A and Bonnet J J 2007 Study of thermal aging effect on space charge in poly(methyl methacrylate) *Eur. Polym. J.* **43** 4821–9
[29] Devikala S, Kamaraj P and Arthanareeswari M 2018 Corrosion resistance behavior of PVA/TiO_2 composite in 3.5% NaCl *Materials Today: Proceedings.* **5** 8672–E

[30] Rajesh Kumar B and Hymavathi B 2017 X-ray peak profile analysis of solid-state sintered alumina doped zinc oxide ceramics by Williamson–Hall and size-strain plot methods *Journal of Asian Ceramic Societies.* **5** 94–103
[31] Klug H P and Alexander L E 1974 *X-ray Diffraction Procedures: for Polycrystalline and Amorphous Materials* 2nd edn (New York: Wiley-VCH)
[32] Vanderschueren J, Aras L, Boonen C, Niezette J and Corapci M 1984 Evidence for clustering in N-butyl methacrylate ionomers as shown by thermally stimulated currents *J. Polym. Sci. Pol. Phys.* **22** 2261–74
[33] Turnhout V J 1975 *J. Electrostat.* **1** 147–61
[34] Chen R and Kirsh Y 1981 *Analysis of Thermally Stimulated Process* (Pergamon Press) Reference book (ISBN: 9781483285511)
[35] Hilezer B and Malecki J 1986 *Electrets, Studies in Electrical and Electronical Engineering* (Amsterdam: Elsevier)
[36] Topic M, Music S and Risti M 2004 Study of relaxation in $Li_2Si_2O_5$ by thermally stimulated depolarization current *Mater. Chem. Phys.* **87** 311–7
[37] Zghal E, Namouchi F and Guermazi H 2014 Study of polarization parameters effect on dipolar relaxation in epoxy-based polymer using thermally stimulated depolarization current *EPJ AP.* **65** 31302–9
[38] Zielinski M and Kryszenski M 1977 Thermal sampling technique for the thermally stimulated discharge in polymers by model calculations *Phys. Status Solidi a* **42** 305 -314
[39] Lacabanne C, Goyaud P and Boyer R F 1980 Thermally Stimulated Current (TSC) study of the Tg and T_{II} transitions in anionic polystyrenes *J. Polym. Sci. Pol. Phys.* **18** 277–84
[40] Belana J, Colomer P, Pujal M and Montserrat S 1985 The glass transition temperature of amorphous poly (ethylene terephthalate) by thermally stimulated currents *J. Macromol. Sci. B.* **23** 467–81
[41] Belana J, Mudarra M, Calaf J, Cañadas J C and Menéndez E 1993 TSC study of the polar and free charge peaks of amorphous polymers *IEEE Zkansactions on Electrical Insulation.* **28** 287–93
[42] Gupta A K, Bajpai R and Keller J M 2011 Transient charging and discharging current study in pure *PVF. B. Mater. Sci.* **34** 105–12
[43] Volkov A S, Koposov G D, Perfil'ev R O and Tyagunin A V 2018 Analysis of experimental results by the Havriliak–Negami model in dielectric spectroscopy *Opt. Spectrosc.* **124** 202–5
[44] Song W B, Wang L Y and Wang Z D 2011 Synthesis and thermomechanical research of shape memory epoxy systems *Mater. Sci. Eng. A* **529** 29–34
[45] Creswell R A and Perlman M M 1970 Thermal currents from corona charged mylar *J. Appl. of P.* **41** 2365–75
[46] Jilani W, Mzabi N, Gallot-Lavallée O, Fourati N, Zerrouki C, Zerrouki R and Guermazi H 2015 Dielectric relaxations investigation of a synthesized epoxy resin polymer *Eur. Phys. J. Plus.* **130** 1–10
[47] Bouzidi A, Omri K, El Mir L and Guermazi H 2015 Preparation, structural and optical investigations of ITO nanopowder and ITO/epoxy nanocomposites *Mat. Sci. Semi. Con. Proc.* **39** 536–43
[48] Moussa S, Namouchi F and Guermazi H 2015 Elaboration, structural and optical investigations of ZnO/epoxy nanocomposites *Eur. Phys. J. Plus.* **130** 1–9
[49] Tauc J 1974 *Amorphous and Liquid Semiconductor* (New York: Plenum) pp. 159
[50] Ho W F, Uddin M A and Chan H P 2009 The stability of high refractive index polymer materials for high-density planar optical circuits *Polym. Degrad. Stab.* **94** 158–61
[51] Bouzidi A, Omri K, Jilani W, Guermazi H and Yahia I S 2018 Effect of the different concentrations of ZnO:Mn incorporation on the microstructure and dielectric properties of epoxy nanocomposites *J. Mater. Sci., Mater. Electron.* **29** 5908–17
[52] Rajesh K, Krishnan P, Mani A, Anandan K, Gayathri K and Devendran P 2019 Physical strength and Opto-electrical conductivity of L-Serine Phosphate single crystal for structural and photonics devices fabrication *Mater. Res. Innovations* 1–7